Self-Assembled Lenalidomide/AIE Prodrug Nanobomb for Tumor Imaging and Cancer Therapy

Mai, Zhijian; Cao, Nengjie; Cheng, Erzhuo; Zeng, Zhiwen; Feng, Yancong; Wang, Yao; French, Paddy J.; Lee, Yi Kuen; Yang, Haihong; More Authors

DOI
10.1021/acsanm.3c03611

Publication date
2023

Document Version
Final published version

Published in
ACS Applied Nano Materials

ACS APPLIED NANO MATERIALS

www.acsanm.org Article

Self-Assembled Lenalidomide/AIE Prodrug Nanobomb for Tumor Imaging and Cancer Therapy

Zhijian Mai,[¶] Nengjie Cao,[¶] Erzhuo Cheng, Zhiwen Zeng, Yancong Feng, Yao Wang,* Paddy J. French, Yi-Kuen Lee, Haihong Yang, Bin Yang,* Hao Li,* and Guofu Zhou

Cite This: *ACS Appl. Nano Mater.* 2023, 6, 19807−19817 Read Online

ACCESS | Metrics & More | Article Recommendations | Supporting Information

ABSTRACT: To develop multifunctional small-molecule prodrugs is highly desirable for cancer treatment but remains challenging in intrinsic traceability. As an acid-cleavable linkage, a Schiff bases benefiting from its distinctive fluorescence quenching ability was selected to prepare a small-molecule prodrug with cancer-targeted and self-indicating. In this study, we designed and developed a multifunctional self-assembled nanobomb of amphiphilic TPE-Lenalidomide prodrug, which comprises a hydrophobic aggregation-induced emission (AIE) probe 4-(1,2,2-triphenylvinyl)benzaldehyde (TPE-CHO) and a hydrophilic anticancer drug Lenalidomide via a Schiff base linkage. We investigated the synergistic effect of d-PET and C═N isomerization which would keep the fluorescence of TPE-Lenalidomide in the "always off" state by density functional theory (DFT) calculation. Once reaching the pathological site, such a vesicular nanobomb of TPE-Lenalidomide will be acidolyzed to release the AIE probe and Lenalidomide molecules simultaneously, consequently realizing high-efficiency effects of tumor imaging and cancer therapy (cell viability: normal cell L929, ∼79.49%; cancer cell 4T1, ∼27.08%; $p = 0.000118$). This work may pave an avenue to prepare small-molecule prodrugs for tumor-targeted diagnosis and cancer therapy.

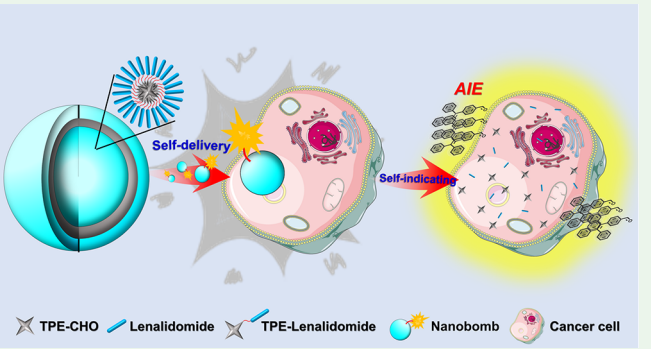

KEYWORDS: *small-molecule prodrug, Schiff base linkage, aggregation-induced emission, self-assembly, tumor-targeted diagnosis and therapy*

INTRODUCTION

Cancer remains as one of the most significant diseases that seriously threatens human health all over the world.[1−3] In order to effectively inhibit malignant tumor and prolong survival, varieties of drug delivery systems and polymer prodrugs have been developed.[4−7] However, most of them are restricted by their low drug loading capacity, and serious cumulative cytotoxicity.[8,9] By comparison, small-molecule prodrugs[9−14] have the advantage of high loading capacity and easy metabolism for cancer therapeutics. Typically, Yan et al.[15] developed an amphiphilic small-molecule prodrug by integrating a hydrophilic anticancer drug and a hydrophobic anticancer drug via a hydrolyzable ester linkage and proposed the concept of amphiphilic drug−drug conjugate (ADDC), which opens up a new way for self-delivery systems. Nevertheless, most small-molecule prodrugs were designed for chemotherapy only. Besides delivering drugs to pathological sites for therapeutic purposes, tumor-targeted imaging, especially real-time imaging, of the tumor locations is also of great significance. Real-time imaging the tumor location and further indicating the organ accumulation of drugs will certainly help understanding the pharmacological effects and then precisely predict the treatment responses.[16,17]

As one of the noninvasive imaging methods, fluorescence imaging has the advantage of long-term tracking and *in situ* visualization of process in living organisms.[18,19] In recent years, aggregation-induced emission (AIE) materials were widely studied by Tang and his colleagues in pharmaceutical field.[18,20−22] Different from aggregation caused quenching (ACQ), AIE compounds show significant fluorescence in the aggregation state because of the restriction of intramolecular motion (RIM).[23] Among them, propeller-shaped molecule tetraphenylethylene (TPE) derivatives, which integrate various advantages including large Stokes shifts, bright emission as aggregates, and multimodification site, are the extraordinary indicator candidates.[24−27] In some particular cases, a few

Received: August 4, 2023
Accepted: September 19, 2023
Published: October 18, 2023

https://doi.org/10.1021/acsanm.3c03611
ACS Appl. Nano Mater. 2023, 6, 19807−19817

Scheme 1. Schematic Illustration of Amphiphilic Small-Molecule Prodrug TPE-Lenalidomide Nanobomb from Fabrication to Self-Assembly at the Nanoscale

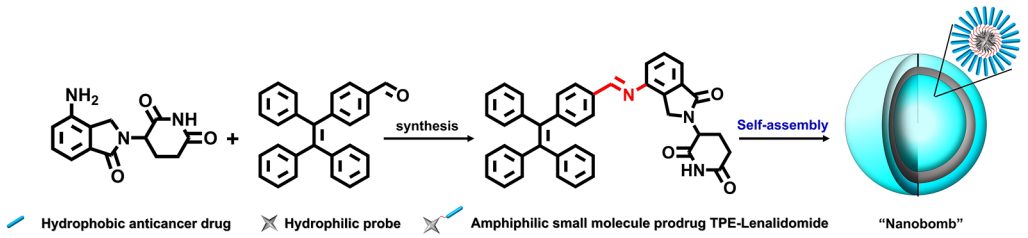

molecules themselves, e.g., doxorubicin,[28] deferasirox,[29] and camptothecin,[15,30] are fluorescent and can serve as an indicator toward specific lesion sites. However, most of available fluorescent small-molecule prodrugs only have "always on" state,[15] which sharply compromises the diagnosis accuracy and therapy safety due to the lack of activatable functions. To date, the most commonly available strategy of preparing theranostic prodrugs is relying on coloading both anticancer drugs and fluorochromes using a polymeric drug delivery carrier. It is still a challenge to develop a small-molecule prodrug to endow prodrug not only with tumor-targeted self-delivery but also with "off-to-on" switchable fluorescence self-indicating.

It is known that some significant changes inside and outside cells will happen when normal cells transform into cancer cells through a complex process.[31−35] One of the typical changes is the increase of acidity around cancer cells, which is because cancer cells have a higher rate of CO_2 production and higher metabolism than normal cells.[34,35] It is reported that extracellular pH values in cancerous tissues is 6.8, and pH values of intracellular compartments such as the endosomes and lysosomes are 4.5−6.5.[36] Therefore, some acid-cleavable linkages such as acetals, hydrazones, esters, ketals, or Schiff bases have been utilized as tumor-targeted components for developing prodrugs.[37−39] With the help of these acid-cleavable linkages, those linked inclusions can be released in the sites of action *in vivo* via the acidolysis reaction. Recently, Wang et al.[40,41] reported that C═N isomerization in Schiff base compounds is the predominant decay process of excited states with an unbridged C═N structure, which would induce the "always off" state of prodrug. Based on this work, Schiff bases, as an acid-cleavable linkage, could become good candidates for precisely manipulating the fluorescence of small-molecule prodrug. That is, once reaching the pathological site, a probe-drug structural prodrug with Schiff base linkage would be acidolyzed and the C═N bond would be broken, along with the fluorescence probe and the anticancer drug releasing.

In this work, a cancer-targeted nanobomb of small-molecule prodrug TPE-Lenalidomide was designed and synthesized through integrating a hydrophilic anticancer drug Lenalidomide[42,43] with a hydrophobic aggregation-induced emission (AIE) probe, 4-(1,2,2-triphenylvinyl)benzaldehyde (TPE-CHO), by a Schiff base linkage (Scheme 1). Owing to its amphiphilic structure, TPE-Lenalidomide could self-assemble into a vesicle for self-delivery. When the nanobomb is "detonated" by more acidic conditions around cancer cells, the quenched fluorescence will rapidly emit, indicating the real-time process of releasing Lenalidomide molecules. This work brings fresh insight into the exploration of versatile nanobombs of small-molecule prodrugs with both functions of self-delivery and self-indication.

EXPERIMENTAL SECTION

Synthesis of TPE-CHO.[47] A 500 mL flask charged with 300 mL of tetrahydrofuran (THF) and 12.8 g of Zn powder (196 mmol) was placed in an ice-salt bath under continuous stirring. Then, $TiCl_4$ was added dropwise under N_2 protection below 0 °C. Consequently, the mixture was stirred at room temperature for 30 min, and then the mixture was refluxed for 3 h. After that, 4 mL of pyridine, 2.0 g of benzophenone (11 mmol), and 2.1 g of 4-benzoylbenzaldehyde (10 mmol) were added into the flask. The reaction continued to reflux for about 1 day. After the reaction mixture cooled to room temperature, the solvent was removed using rotary evaporation. The residue was added to water and extracted twice with dichloromethane (DCM). Finally, the obtained mixture was purified by column chromatography using DCM/PE (1/3, V/V) as eluent. The target molecular 4-(1,2,2-triphenylvinyl)benzaldehyde (TPE-CHO) was obtained in about 45% yield based on benzophenone. ^{1}H NMR (600 MHz, chloroform-*d*) δ 9.93 (s, 1H), 7.65 (d, 2H), 7.24 (d, 2H), 7.11 (m, 15H). Q-Exactive LC-MS calcd for $[M + H]^+$: 361.15869. Found: 361.15891. ^{1}H NMR, ^{13}C NMR and mass spectra of TPE-CHO were shown in Figures S1−S3, respectively.

Synthesis of TPE-Lenalidomide.[36] A portion of TPE-CHO (0.1 g, 0.28 mmol), Lenalidomide (0.1 g, 0.39 mmol), formic acid (50 μL), and 30 mL of ethanol were combined into the flask. The mixture was stirred under reflux conditions overnight. Then, solvent was removed under reduced pressure, followed by chromatography using a silica gel column (PE: EA, 2:1, v:v). The product was further heated at 65 °C under high vacuum for 4 h to afford TPE-Lenalidomide as a yellow solid in about 50% yield based on TPE-CHO. ^{1}H NMR (600 MHz, DMSO-d_6) δ 10.98 (s, 1H), 8.64 (s, 1H), 7.74 (d, 2H), 7.60 (d, 2H), 7.45 (s, 1H), 7.15 (m, 12H), 7.01 (m, 5H), 5.13 (t, 1H), 4.47 (s, 1H), 4.35 (d, 1H), 2.91 (q, 1H), 2.57 (q, 1H), 2.44 (q, 1H), 1.98 (q, 1H). Q-Exactive LC-MS calcd for $[M + H]^+$: 602.24381. Found: 602.24408. ^{1}H NMR, ^{13}C NMR and mass spectra of TPE-CHO were shown in Figures S4−S6, respectively.

Preparation of TPE-Lenalidomdie Nanobomb. In brief, about 6 mg of TPE-Lenalidomide was dissolved in 1 mL of dimethyl sulfoxide (DMSO) and stirred at room temperature for 1 min to produce a solution with a concentration of 10^{-2} mol/L. Then, 0.03 mL of solution was slowly added to 2.97 mL of deionized water or PBS with different pH values (pH = 7.4, 6.0, 5.5, and 5.0) for further experiments, respectively.

CMC Measurement.[12] To investigate the self-assembly in nanoscale behavior of TPE-Lenalidomide in water, the critical micelle concentration (CMC) was measured by using pyrene as a fluorescent probe (Figure S7). The fluorescence intensities of the first (I_1) and third (I_3) bands of pyrene are sensitive to the surrounding medium. When the concentration of TPE-Lenalidomide was less than 10 μg/mL, the I_1/I_3 value remained nearly unchanged. Once the concentration of TPE-Lenalidomide reached the characteristic level of pyrene in a hydrophobic environment, the ratio of I_1/I_3 started to increase dramatically. According to the fitted curves, the CMC value of the TPE-Lenalidomide is about 13.60 μg/mL.

Density Functional Theory (DFT) Calculation. The molecular structure map was plotted by GaussView 6.0.16.[48] The geometry optimization and frequency analyses were finished via density functional theory (DFT) with the M06-2X exchange−correlation

https://doi.org/10.1021/acsanm.3c03611
ACS Appl. Nano Mater. 2023, 6, 19807−19817

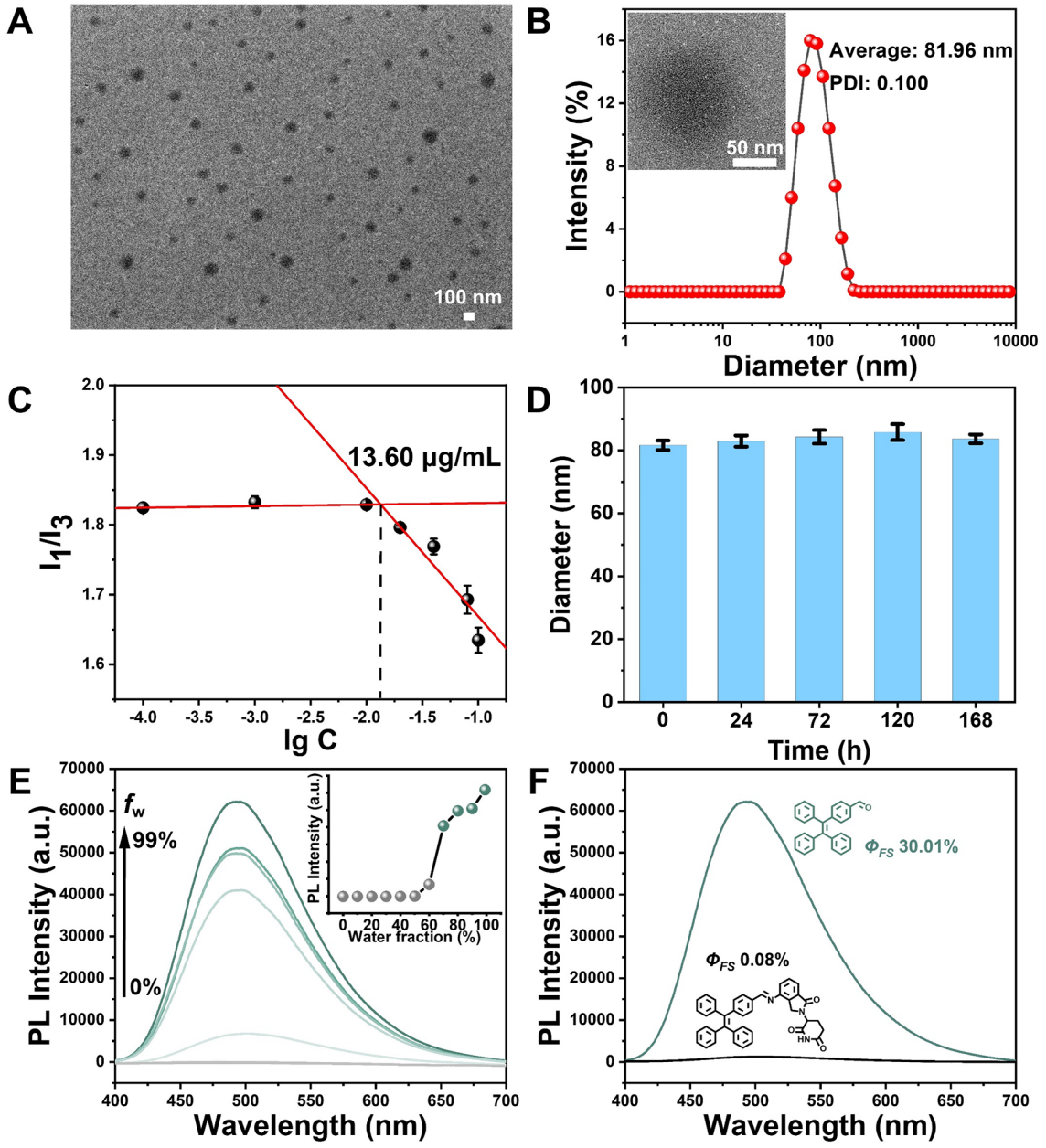

Figure 1. (A) TEM image of TPE-Lenalidomide nanobomb formed in DMSO/water mixture with f_w = 99 vol %. (B) DLS measurement of the TPE-Lenalidomide nanobomb. The polydispersity index is about 0.100. Inset: the amplified image of a nanoparticle. (C) Relationship between the fluorescence intensity ratio (I_1/I_3) and TPE-Lenalidomide concentration. The CMC value is about 13.60 μg/mL. (D) Time-dependent stability of the TPE-Lenalidomide nanobomb. (E) PL spectra of TPE-CHO (10^{-4} M) in DMSO/H_2O with different fractions of water (f_w). Inset: maximum emission peak of TPE-CHO (10^{-4} M) at 500 nm versus water fraction. (F) PL spectra of TPE-CHO (10^{-4} M) and TPE-Lenalidomide (10^{-4} M) in DMSO/H_2O (V/V 1:99).

functional[49] in conjunction with the def2-TZVP basis set[50] in *N*,*N*-dimethylformamide. To give direct information on the C═N isomerization, the constrained energy profiles of *trans*-TPE-Lenalidomide varying with dihedral angle C−C−N−C were explored via time-dependent (TDDFT) with the B3LYP exchange−correlation functional[51] in conjunction with the 6-31G(d) basis set[52] in a vacuum. All calculations were performed using the Gaussian 16 C.01 code.[53] The isosurface maps of the article were rendered by virtue of the VMD visualization program[54] based on the files exported by Multiwfn 3.7 code.[55]

Culture Conditions. Mouse breast cancer cells (4T1) were cultured in DMEM medium with high sugar containing 10% FBS and 1% penicillin-streptomycin; mouse epithelioid fibroblasts (L929) were cultured in MEM medium containing 10% FBS and 1% penicillin-streptomycin. The incubator temperature was 37 °C and the CO_2 content was 5%.

***In Vitro* Cellular Uptake.** 4T1 cells and L929 cells were inoculated at a cell density of 50,000/dish and cultured overnight in confocal dishes, and then the prepared TPE-CHO and TPE-Lenalidomide were added to the dishes and incubated for 1.5, 6, and 24 h in the medium of pH 7.4 and 5.0, respectively. Then the medium was aspirated off and washed with PBS buffer, DAPI solution (1 μg/mL) was added and incubated, and finally the cells were washed with PBS buffer and observed using a confocal laser scanning microscopy (Zeiss LSM 980) with the excitation wavelengths of 488 nm for TPE-CHO and 405 nm for DAPI, respectively.

***In Vitro* Cytotoxicity.** The 4T1 cells and L929 cells were inoculated in 96-well plates at a cell density of 8000/well overnight,

https://doi.org/10.1021/acsanm.3c03611
ACS Appl. Nano Mater. 2023, 6, 19807−19817

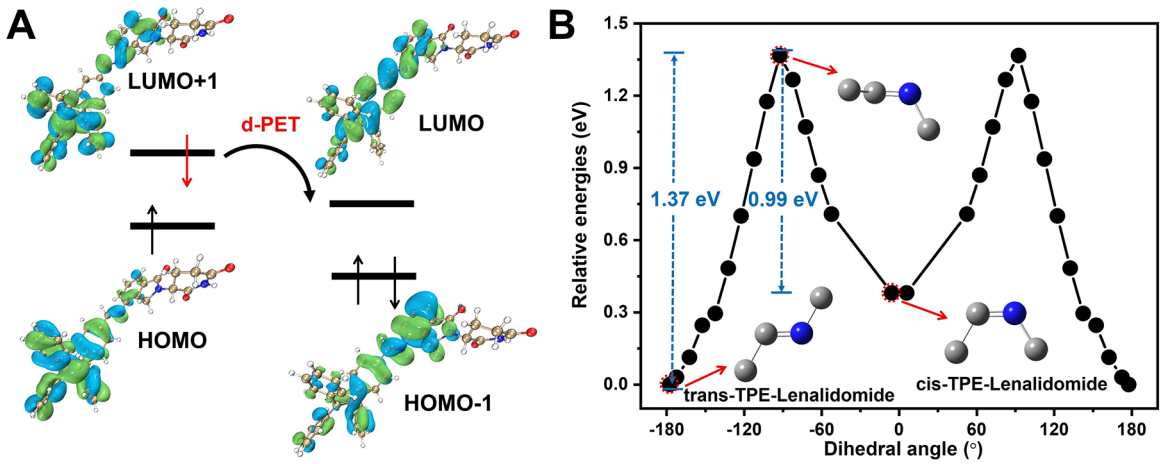

Figure 2. (A) Schematic of the signaling mechanism of the d-PET effect. Carbon, nitrogen, oxygen, and hydrogen atoms are colored in golden, blue, red, and white, respectively. (B) The potential energy curve of the dihedral angle C−C−N−C of the *trans*-TPE-Lenalidomide form to the *cis*-TPE-Lenalidomide form. Carbon and nitrogen are colored in gray and blue, respectively.

and the prepared Lenalidomide, TPE-CHO, and TPE-Lenalidomide were sterilized and added to the corresponding medium with different gradient concentrations at a volume of 100 μL per well and then incubated for 48 h. After that, the medium was aspirated, 100 μL of MTT solution with a concentration of 0.5 mg/mL was added to each well, and the incubation was continued for 4 h. Finally, the MTT solution was aspirated, 150 μL of DMSO solution was added to each well, and the cell viability was calculated by measuring the absorbance value at 490 nm using a microplate reader (Synergy H1). The calculation formula was as follows:

$$\text{Cell viability (\%)} = (\text{As} - \text{Ab})/(\text{Ac} - \text{Ab}) \times 100\%$$

where As is the absorbance of samples wells, Ac is the absorbance of control wells, and Ab is the absorbance of blank wells. Data are shown as means ± standard deviation (SD) on the basis of independent experiments.

RESULTS AND DISCUSSION

Construction and Characterizations of TPE-Lenalidomide. In this case, a multifunctional TPE derivative TPE-Lenalidomide was designed and prepared through nucleophilic addition (Scheme S1), and the details are described in the Experimental Section. The chemical structure and molecular weight of TPE-CHO and TPE-Lenalidomide were fully characterized by ^{1}H and ^{13}C nuclear magnetic resonance spectroscopy and mass spectrometry (Figures S1−S6).

TPE-Lenalidomide was designed as an amphiphilic structure (Figure S7), which would endow it with the ability to self-assemble for self-delivery. As shown in Figure 1C, the critical micelle concentration (CMC) is about 13.60 μg/mL, which confirms that the inherent amphiphilicity of TPE-Lenalidomide provides the ability for itself to form self-assembly in nanoscale. Moreover, the size and morphology of TPE-Lenalidomide nanobomb are confirmed by transmission electron microscopy (TEM). As expected, the TPE-Lenalidomide "nanobombs" have a spherical shape, with an average size of 88.82 nm (Figure 1A). According to dynamic light scattering (DLS) particle size analysis (Figure 1B), average hydrodynamic diameter of TPE-Lenalidomide (10^{-4} M) is approximate 81.96 nm, which is close to the TEM measurement. No significant change in diameter of TPE-Lenalidomide nanobomb was observed at different time intervals within 1 day, which demonstrates that TPE-Lenalidomide nanobomb is suitable for *in vivo* drug metabolism (Figure 1D).

The fluorescence properties of TPE-Lenalidomide and its precursor TPE-CHO were confirmed by PL spectra. As shown in Figure 2E, TPE-CHO presents as highly emissive and its fluorescence intensity gradually increases with the growth of the volume fraction of water (f_w) in DMSO/H_2O. When water fraction is less than 60%, TPE-CHO is almost nonfluorescent. Once the water fraction increases from 60% to 99%, the fluorescence intensity dramatically increases. Once the water fraction reaches 99%, the fluorescence intensity of TPE-CHO is nearly 82-fold stronger than that of pure DMSO, which reveals that TPE-CHO is a typical AIE type molecule. On the contrary, TPE-Lenalidomide is almost nonfluorescent even if the water fraction reaches 99% (Figure S8). The fluorescence intensity of TPE-CHO was nearly 48-fold stronger than that of TPE-Lenalidomide in the same water fraction (f_w = 99%, Figure 2F). The PL quantum yield of TPE-CHO in the solid state is found to be 30.31%, and TPE-Lenalidomide is almost nonfluorescent (Φ_{FS} 0.08%). Obviously, the above results demonstrate that the fluorescence of the TPE unit was quenched after Lenalidomide was modified to TPE-CHO via Schiff base linkage.

DFT Calculation of Signaling Mechanism. In order to get deep insight into the signaling mechanism of Schiff base compounds, we verified the possible PET effect and energy consumption during C═N isomerization in TPE-Lenalidomide by DFT calculations. The selective electron transition energies, oscillator strength, and configuration interaction contributions of TPE-Lenalidomide are reported in Table 1. Interestingly, oscillator strengths for the absorption to the S_3 state (HOMO → LUMO+1) are large (f = 0.3928). The LUMO and LUMO+1 of TPE-Lenalidomide mainly distribute in the fluorophore TPE unit (electron donor) and the receptor

Table 1. Selective Electron Transition Energies, Oscillator Strength (f), and Configuration Interaction (CI) Contributions (Major MO Involvement, %) of *trans*-TPE-Lenalidomide

Transition	Energy (eV)	f	CI contributions (%)
$S_0 \rightarrow S_1$	3.70 (335 nm)	1.03	H → L (83.2)
$S_0 \rightarrow S_2$	4.14 (300 nm)	0.12	H−1 → L (43.2), H → L+1 (14.7)
$S_0 \rightarrow S_3$	4.69 (264 nm)	0.39	H → L+1 (58.6)

https://doi.org/10.1021/acsanm.3c03611
ACS Appl. Nano Mater. 2023, 6, 19807−19817

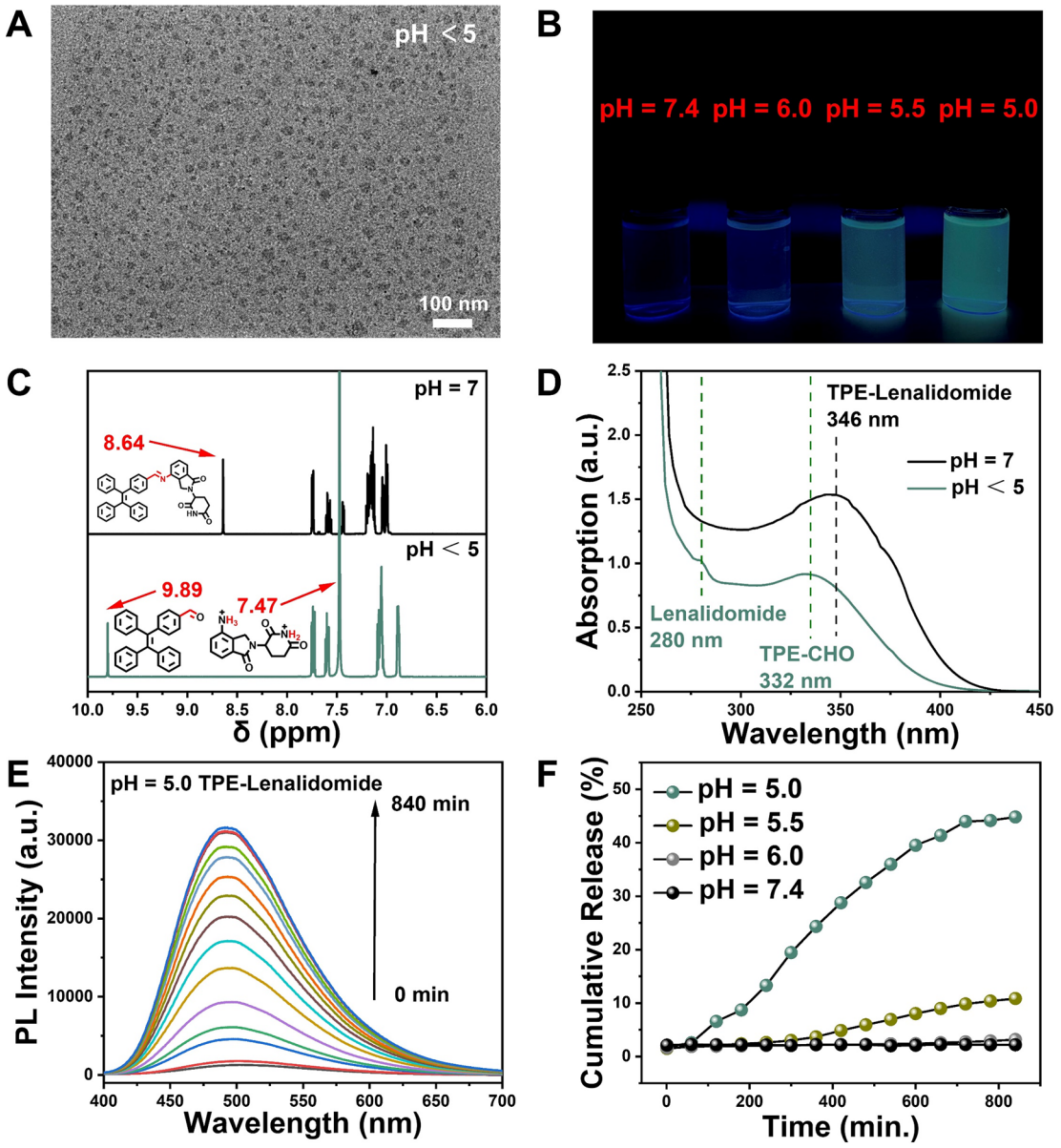

Figure 3. (A) TEM image of TPE-Lenalidomide nanobomb after immersion in DMSO/H_2O (V/V 1:99) with pH = 5.0 for 15 h. (B) Photograph of TPE-Lenalidomide under UV lamp (365 nm) after 15 h in PBS buffer solutions with different pH (7.4, 6.0, 5.5, and 5.0) values. (C) ^{1}H NMR image of TPE-Lenalidomide in DMSO-*d* and DMSO-*d*/HCl-*d*. (D) UV−vis spectra of TPE-Lenalidomide (10^{-4} M) in DMSO or DMSO/HCl. (E) Time-dependent PL spectra of TPE-Lenalidomide in pH = 5.0 PBS buffer solutions. (F) Accumulated release profiles of Lenalidomide from TPE-Lenalidomide under different pH values according to fluorescence intensity change.

Lenalidomide unit (electron acceptor), indicating that the excited state electron could transfer from the TPE unit to the Lenalidomide unit. Because the excited electrons from the $S_0 \rightarrow S_3$ transition quickly relaxed via internal conversion to the S_1 state and due to the charge transfer nature of the $S_1 \rightarrow S_0$ transition, the S_0 state is blocked and results in weak fluorescence (Figure 2A). This type of signaling mechanism is called donor-excited photoinduced electron transfer (d-PET).[44−46]

Furthermore, the potential energy curve of the dihedral angle C−C−N−C in TPE-Lenalidomide is shown in Figure 2B. Since the potential energy of *trans*-TPE-Lenalidomide is lower than that of *cis*-TPE-Lenalidomide, the transition from *trans*-TPE-Lenalidomide to *cis*-TPE-Lenalidomide requires crossing an energy barrier (1.37 eV), which means that, as a dynamic molecular conformational motion, the unhindered C═N isomerization would consume the energy of excited states and results in weak emission. All the above calculated results indicate that the synergistic effect of the d-PET and C═N isomerization keeps the fluorescence of TPE-Lenalidomide in the "always off" state.

Characterizations of Drug Release and Fluorescence Turn-On. To investigate the pH responsive ability of the TPE-Lenalidomide nanobomb, the structure change under neutral and acidic conditions was confirmed by TEM, ^{1}H NMR, and UV−vis spectra. TPE-Lenalidomide was immersed into acidic solution with pH = 5.0, and the structural biodegradation process was revealed by TEM images. As depicted in Figure 3A, after about 15 h, the morphology of the TPE-Lenalidomide nanobomb was seriously etched and collapsed,

https://doi.org/10.1021/acsanm.3c03611
ACS Appl. Nano Mater. 2023, 6, 19807−19817

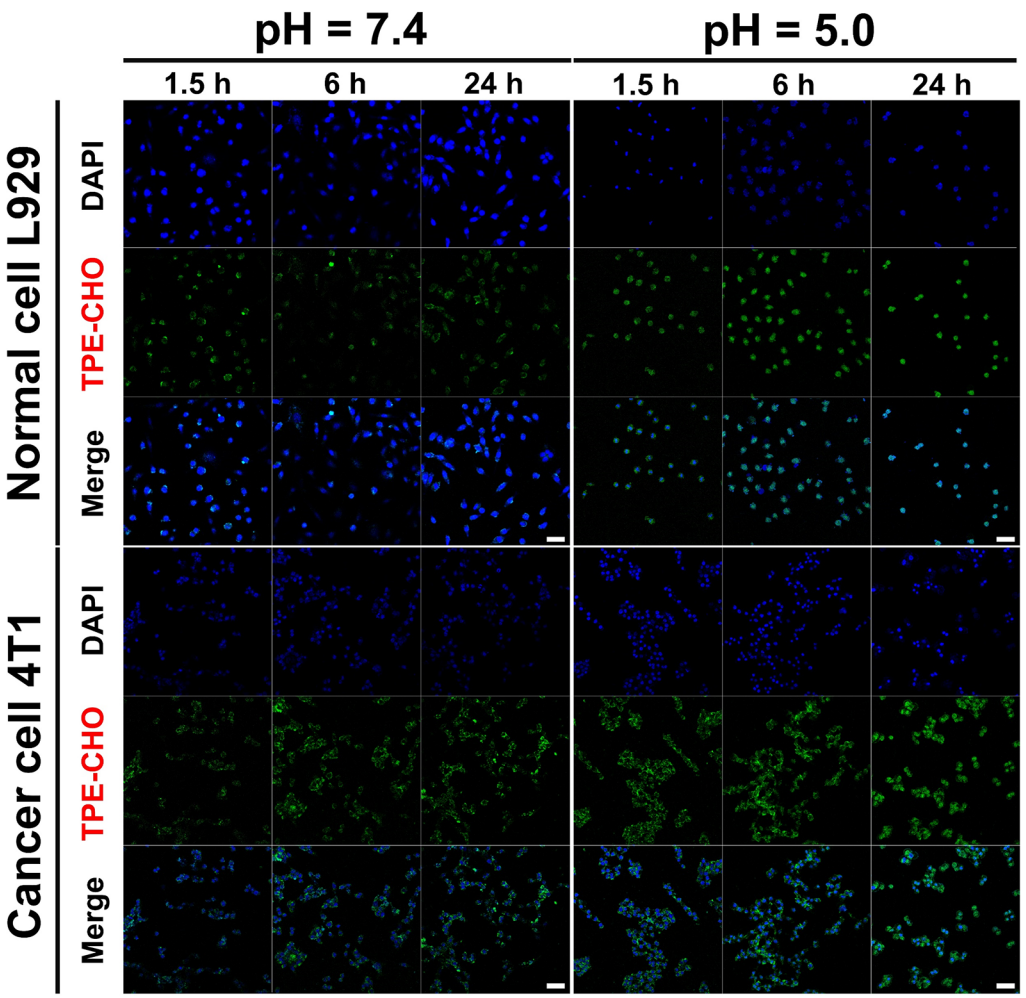

Figure 4. CLSM images of L929 or 4T1 cells after incubation with 1 mL of TPE-CHO (66.5×10^{-12} mol/L) for 1.5, 6, and 24 h at 37 °C, respectively. Scale bar: 50 μm.

which may be ascribed to the disassembly under higher acidic condition. Furthermore, as shown in Figure 3C, the chemical shift at 8.64 ppm assigned to the Schiff base linkage of TPE-Lenalidomide in DMSO-*d*. After a moderate amount of HCl-*d* was used to adjust the pH value to enable the complete decomposition of TPE-Lenalidomide, the proton signals of the formyl group and ammonium ion at 9.89 and 7.47 ppm emerged, and the signal of the Schiff base at 8.64 ppm disappeared, which indicated that TPE-Lenalidomide decomposed into TPE-CHO and Lenalidomide under acidic condition. The UV−vis measurement was used to further confirm the pH responsive process of TPE-Lenalidomide (Figure 3D). Compared to the UV−vis absorption of TPE-Lenalidomide at 345 nm, two new absorption peaks at 280 and 332 nm are found after the addition of trace amounts of hydrochloric acid. The absorption peak at 280 nm is ascribed to the anticancer drug Lenalidomide, and the absorption peak at 332 nm belongs to TPE-CHO in the same condition. Both ^{1}H NMR and UV−vis measurements demonstrate that TPE-Lenalidomide would be acidolyzed and immediately break the C═N bond, along with the fluorescence probe and the anticancer drug releasing under acidic pH condition.

To further investigate the "off-to-on" fluorescently self-indicating process, the fluorescence property of TPE-Lenalidomide was studied under different pH conditions. As shown in Figure 3B, the fluorescence change of TPE-Lenalidomide is most pronounced at pH = 5.0 because of the release of TPE-CHO. After about 13 h, the fluorescence intensity at pH = 5.0 tends to be stable and is nearly 24.7-fold stronger than that in the initial state (Figure 3E). Moreover, according to the above research results, the release profile of the anticancer drug Lenalidomide could be constructed by measuring the maximum emission peak of released TPE-CHO at about 500 nm. As shown in Figure 3F, Lenalidomide release at pH = 5.0 is 44.8%, while that at pH = 5.5 is 10.8%, at pH = 6.0 is only 3.2%, and at pH = 7.4 is almost unchanged. It is firmly believed that the prodrug TPE-Lenalidomide could be stable under physiological conditions but releases fluorescence probe TPE-CHO and anticancer drug Lenalidomide simultaneously for "off-to-on" fluorescently self-indicating drug release in tumorous microenvironment after being internalized by cancer cells.

***In Vitro* Experiment of TPE-Lenalidomide for Drug Release Imaging.** In the cell uptake assay, the two small-molecule prodrugs, TPE-Lenalidomide and its precursor TPE-CHO, were evaluated by comparison of the drug entrapment into normal and cancer cells. Obviously, TPE-CHO is absolutely hydrophobic and lacks any responsive capability to the cellular microenvironment. Just as shown in Figure 4 and Figure S9, both the coincubating time and the ambient pH

https://doi.org/10.1021/acsanm.3c03611
ACS Appl. Nano Mater. 2023, 6, 19807−19817

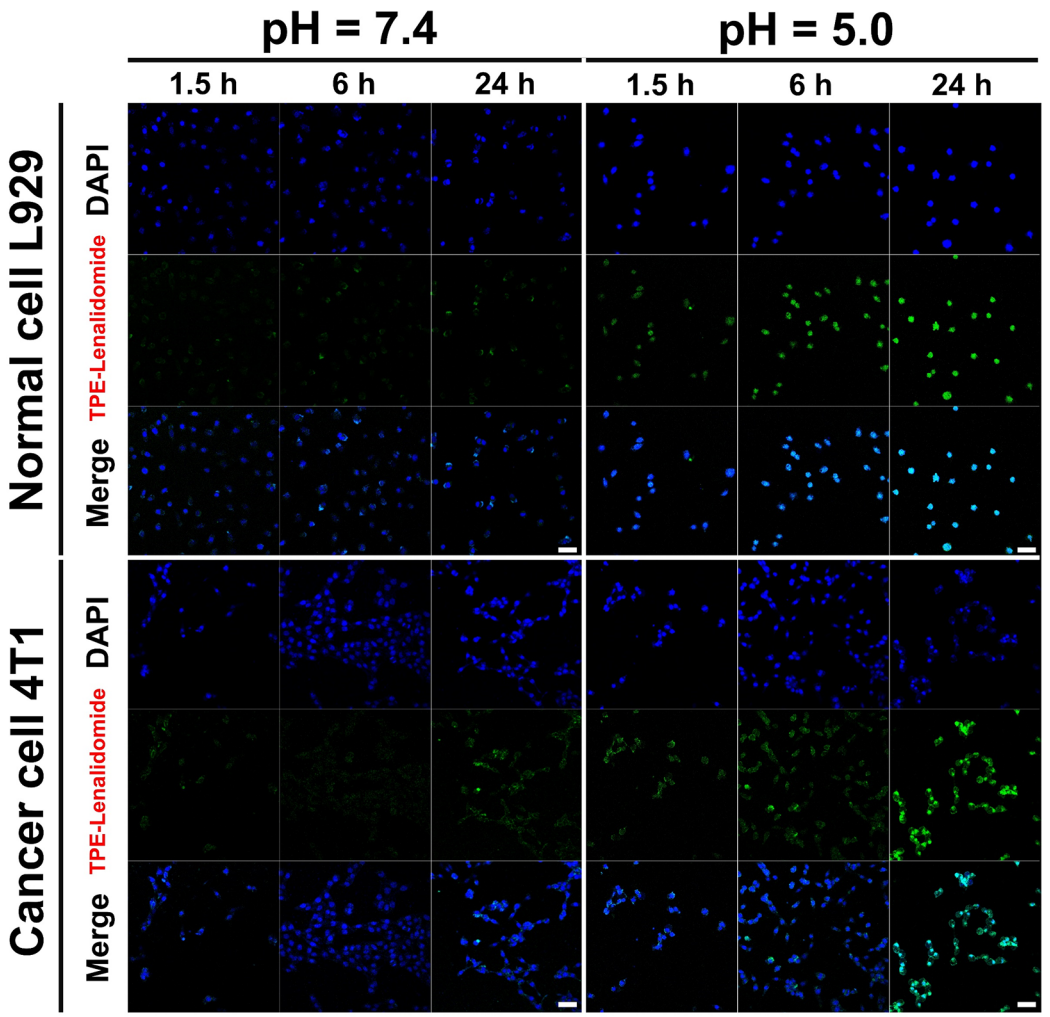

Figure 5. CLSM images of L929 or 4T1 cells after incubation with 1 mL of TPE-Lenalidomide (66.5×10^{-12} mol/L) for 1.5, 6, and 24 h at 37 °C, respectively. Scale bar: 50 μm.

value do not significantly change the uptake effect of TPE-CHO. The only difference is that the uptake rate of TPE-CHO in the cancer cells 4T1 is much higher than the one in the normal cells L929. This may be ascribed to the vigorous metabolism of the cancer cells. After covalent conjugation with Lenalidomide by the Schiff base, TPE-Lenalidomide was newly endowed with amphiphilicity, acid-sensitivity, and specific pharmaceutical effect. Figure 5 and Figure S10 exhibit that more and more green fluorescence clusters originating from the disrupted TPE-Lenalidomide nanobomb of prodrugs are entrapped in the cells along with the prolonged coincubating time, especially to the low pH condition and the cancer cell. Typically at normal physiological pH value, TPE-Lenalidomide rarely entered into the target cells even if coincubated for 24 h. And in the acidic surrounding, more stacked TPE units with green fluorescence are apparently entrapped in the cell nucleus. This phenomenon is further enhanced in the 4T1 cell, in which those green clusters spread over both the cell nucleus and cytoplasm. Since nanoparticles were generally uptaken by cells *via* endocytosis pathway and subsequently transported to endosomes/lysosomes, finally reached the nucleus region, it can be speculated from the drug releasing results (Figure 3F) that intracellular acidic stimuli of cancer cells plays an important assisting role in the breakage and following emission of TPE-Lenalidomide. The specific cancer-targeting ability of TPE-Lenalidomide is also demonstrated.

***In Vitro* Experiment of TPE-Lenalidomide for Cancer Therapy.** Just as mentioned above, the AIE imaging of the TPE units in the aqueous environment simultaneously accompanies the release of Lenalidomide units during the acidolysis of TPE-Lenalidomide. To nonresponsive oil-soluble TPE-CHO, there is no significant difference in the cell viability for the normal and cancer cells (L929, ~61.30%; 4T1, ~62.38%) (Figure 6A). As the crude model drug, water-soluble Lenalidomide exhibits positive toxicity for 4T1 cells (cell viability: ~32.67%) after 48 h incubation when the concentration is about 66.5×10^{-12} mol/L. On the contrary, it shows low toxicity for L929 cells (cell viability: ~70.99%; p = 0.000636; Figure 6B). Similarly, amphiphilic TPE-Lenalidomide also behaves with a huge difference in the cell viability (L929, ~79.49%; 4T1, ~27.08%; p = 0.000118; Figure 6C). According to the above analysis (see Figure 6D), this pharmacological action takes the pharmaceutical effect of Lenalidomide to the most extent, which is mainly attributed to the response of TPE-Lenalidomide to the tumorous microenvironment.

Diagnosis and Therapy Mechanism of TPE-Lenalidomide. The mechanism of cancer-targeted diagnosis and cancer therapy is shown in Scheme 2. Ascribing to the amphiphilic

https://doi.org/10.1021/acsanm.3c03611
ACS Appl. Nano Mater. 2023, 6, 19807−19817

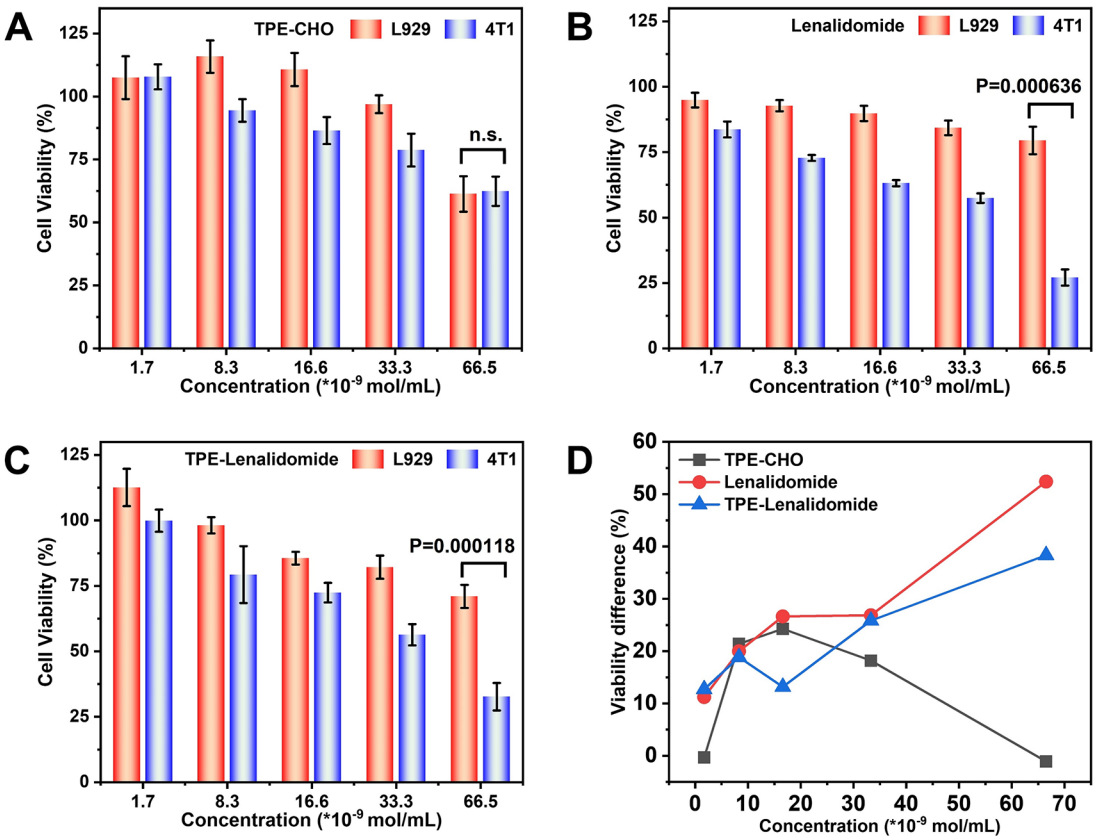

Figure 6. Cell viabilities of L929 cells and 4T1 cells after incubation with different concentrations of (A) TPE-CHO, (B) Lenalidomide, and (C) TPE-Lenalidomide for 48 h. (D) Viability difference between normal cell L929 and cancer cell 4T1 after incubation with different concentrations of TPE-CHO, Lenalidomide, and TPE-Lenalidomide.

Scheme 2. Imaging and Therapy Mechanism of TPE-Lenalidomide Nanobomb of Prodrug

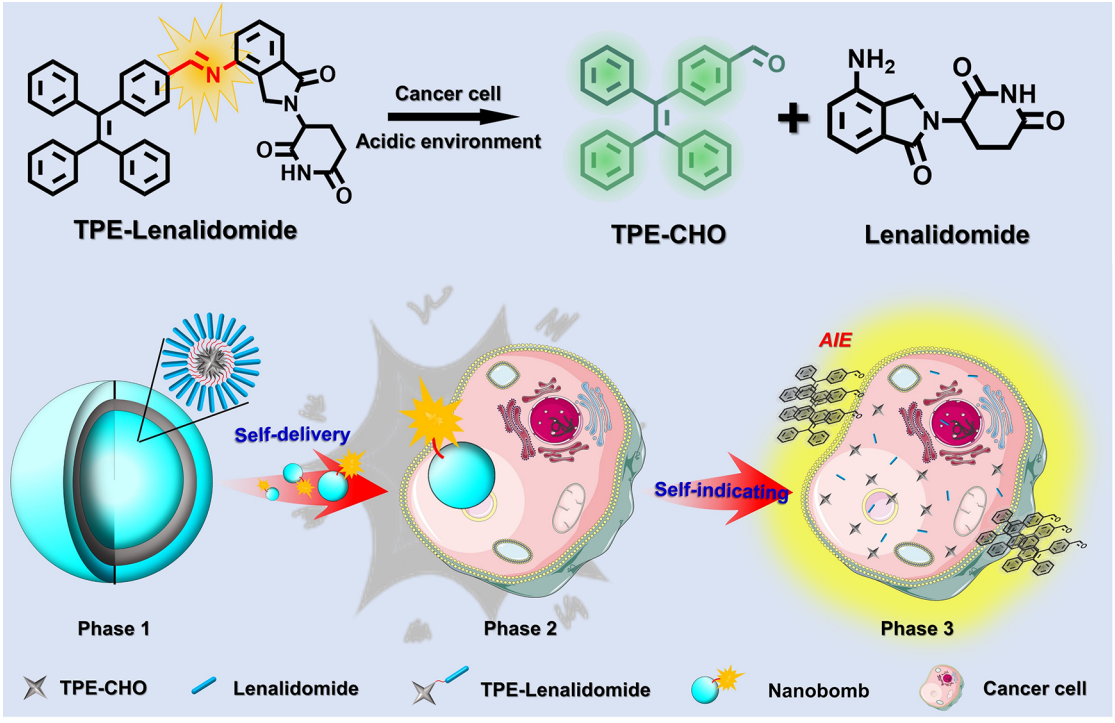

structure, the small-molecule prodrug TPE-lenalidimide can self-assemble into a nanobomb to deliver itself into tumor tissues (phase 1 and phase 2). After the cellular internalization of the nanobomb, the Schiff base linkage would be hydrolyzed

https://doi.org/10.1021/acsanm.3c03611
ACS Appl. Nano Mater. 2023, 6, 19807−19817

and the fluorescence quenching effect of C=N isomerization is no longer applicable. Both the free fluorescence probe TPE-CHO and the anticancer drug Lenalidomide can simultaneously be released to indicate the drug delivery process and to attack the cancer cells for potential cancer-targeted diagnosis and cancer therapy (phase 3).

CONCLUSIONS

In summary, we integrated a hydrophobic AIE probe and a hydrophilic anticancer drug into an amphiphilic TPE-Lenalidomide prodrug via a Schiff base linkage. The results show that the probe-drug structural TPE-Lenalidomide molecules can self-assemble into spherical nanobombs with the size of about 82 nm and behave by increasing its own fluorescence intensity in a low pH environment. According to the *in vitro* experiments, TPE-Lenalidomide exhibited huge variation in fluorescence intensity and positive toxicity for cancer cells (cell viability: normal cell L929, ~79.49%; cancer cell 4T1, ~27.08%; $p = 0.000118$). We hope that this facile and versatile strategy is of high applied value to design and prepare probe-drug structural small-molecule prodrugs via a Schiff base linkage for cancer-targeted theranostics.

ASSOCIATED CONTENT

Supporting Information

The Supporting Information is available free of charge at https://pubs.acs.org/doi/10.1021/acsanm.3c03611.

Materials and instrumentation, ^{1}H NMR, ^{13}C NMR, and mass spectra of TPE-CHO and TPE-Lenalidomide; aqueous solubility of TPE-CHO and Lenalidomide with different pH values; PL spectra of TPE-Lenalidomide (10^{-4} M) in DMSO/H_2O with different fractions of water (fw); relative fluorescence intensity per pixel of L929 or 4T1 cells after incubation with 1 mL of TPE-CHO and TPE-Lenalidomide (66.5×10^{-12} mol/L) for 1.5, 6, and 24 h at 37 °C (PDF)

AUTHOR INFORMATION

Corresponding Authors

Yao Wang − *Guangdong Provincial Key Laboratory of Optical Information Materials and Technology, Institute of Electronic Paper Displays, South China Academy of Advanced Optoelectronics and National Center for International Research on Green Optoelectronics, South China Normal University, Guangzhou 510006, P. R. China;* orcid.org/0000-0002-0713-5018; Email: wangyao@m.scnu.edu.cn

Bin Yang − *The Sixth Affiliated Hospital of Guangzhou Medical University, Qingyuan People's Hospital; School of Biomedical Engineering, Guangzhou Medical University, Guangzhou 511436, P. R. China;* orcid.org/0000-0001-9416-3094; Email: bjrf2009@sina.com

Hao Li − *Guangdong Provincial Key Laboratory of Optical Information Materials and Technology, Institute of Electronic Paper Displays, South China Academy of Advanced Optoelectronics and National Center for International Research on Green Optoelectronics, South China Normal University, Guangzhou 510006, P. R. China*; Email: haoli@m.scnu.edu.cn

Authors

Zhijian Mai − *Guangdong Provincial Key Laboratory of Optical Information Materials and Technology, Institute of Electronic Paper Displays, South China Academy of Advanced Optoelectronics and National Center for International Research on Green Optoelectronics, South China Normal University, Guangzhou 510006, P. R. China*

Nengjie Cao − *Guangdong Provincial Key Laboratory of Optical Information Materials and Technology, Institute of Electronic Paper Displays, South China Academy of Advanced Optoelectronics and National Center for International Research on Green Optoelectronics, South China Normal University, Guangzhou 510006, P. R. China*

Erzhuo Cheng − *The Sixth Affiliated Hospital of Guangzhou Medical University, Qingyuan People's Hospital; School of Biomedical Engineering, Guangzhou Medical University, Guangzhou 511436, P. R. China*

Zhiwen Zeng − *Guangdong Provincial Key Laboratory of Optical Information Materials and Technology, Institute of Electronic Paper Displays, South China Academy of Advanced Optoelectronics and National Center for International Research on Green Optoelectronics, South China Normal University, Guangzhou 510006, P. R. China*

Yancong Feng − *Guangdong Provincial Key Laboratory of Optical Information Materials and Technology, Institute of Electronic Paper Displays, South China Academy of Advanced Optoelectronics and National Center for International Research on Green Optoelectronics, South China Normal University, Guangzhou 510006, P. R. China*

Paddy J. French − *BE Laboratory, EWI, Delft University of Technology, Delft 2628CD, The Netherland*

Yi-Kuen Lee − *Department of Mechanical & Aerospace Engineering and Department of Electronic & Computer Engineering, Hong Kong University of Science and Technology, Kowloon 999077, P. R. China*

Haihong Yang − *Department of Thoracic Oncology, State Key Laboratory of Respiratory Diseases, The First Affiliated Hospital of Guangzhou Medical University, Guangzhou 510006, P. R. China*

Guofu Zhou − *Guangdong Provincial Key Laboratory of Optical Information Materials and Technology, Institute of Electronic Paper Displays, South China Academy of Advanced Optoelectronics and National Center for International Research on Green Optoelectronics, South China Normal University, Guangzhou 510006, P. R. China;* orcid.org/0000-0003-1101-1947

Complete contact information is available at: https://pubs.acs.org/10.1021/acsanm.3c03611

Author Contributions

[¶]Z.M. and N.C. contributed equally to this work. Z.M. and Y.W. conceived and designed the research. Z.Z. assisted with molecules synthesized and contributed to TEM characterization. N.C. and Y.C. performed the DFT calculation. B.Y. and E.C. contributed to *in vitro* experiments. Y.L., P.J.F., H.Y., B.Y., H.L., and G.Z. helped analyze the data and polish the manuscript. Z.M. and Y.W. wrote the manuscript with input from all authors. All authors discussed, revised, and approved the manuscript.

Notes

The authors declare no competing financial interest.

ACKNOWLEDGMENTS

This work was supported by the National Natural Science Foundation of China (Grant No. 51973070, 51903062),

Science and Technology Program of Guangzhou (No. 2019050001 and 202102020757), Guangdong Basic and Applied Basic Research Foundation (No. 2022A1515010577, 2021A1515012420, 2021A1515010596), Innovative Team Project of Education Bureau of Guangdong Province (2018KCXTD009), Guangdong Science and Technology Project-International Cooperation (2022A0505050069), Start-up Foundation from SCNU, Guangdong Provincial Key Laboratory of Optical Information Materials and Technology (No. 2017B030301007), MOE International Laboratory for Optical Information Technologies, the 111 Project, Science and Technology Innovation Strategy Special Foundation of Guangdong (No. pdjh2023b0144). The calculation of this work was performed on Bianshui Riverside Supercomputing Center (BRSC).

REFERENCES

(1) Dunn, G.; Old, L.; Schreiber, R. The Immunobiology of Cancer Immunosurveillance and Immunoediting. *Immunity* **2004**, *21* (2), 137−148.
(2) Jones, P.; Baylin, S. The Epigenomics of Cancer. *Cell* **2007**, *128* (4), 683−692.
(3) Lujambio, A.; Lowe, S. The Microcosmos of Cancer. *Nature* **2012**, *482* (7385), 347−355.
(4) Cheng, X.; Gao, J.; Ding, Y.; Lu, Y.; Wei, Q.; Cui, D.; Fan, J.; Li, X.; Zhu, E.; Lu, Y.; Wu, Q.; Li, L.; Huang, W. Multi-Functional Liposome: A Powerful Theranostic Nano-Platform Enhancing Photodynamic Therapy. *Adv. Sci.* **2021**, *8*, 2100876.
(5) Jaymand, M. Chemically Modified Natural Polymer - Based Theranostic Nanomedicines: Are They The Golden Gate Toward a de Novo Clinical Approach Against Cancer? *ACS Biomater. Sci. Eng.* **2020**, *6*, 134−166.
(6) Xin, K.; Li, M.; Lu, D.; Meng, X.; Deng, J.; Kong, D.; Ding, D.; Wang, Z.; Zhao, Y. Bioinspired Coordination Micelles Integrating High Stability, Triggered Cargo Release, and Magnetic Resonance Imaging. *ACS Appl. Mater. Interfaces* **2017**, *9*, 80−91.
(7) Borlan, R.; Focsan, M.; Perde-Schrepler, M.; Soritau, O.; Campu, A.; Gaina, L.; Pall, E.; Pop, B.; Baldasici, O.; Claudia, G.; Stoia, D.; Maniu, D.; Astilean, S. Antibody-Functionalized Theranostic Protein Nanoparticles for the Synergistic Deep Red Fluorescence Imaging and Multimodal Therapy of Ovarian Cancer. *Biomater. Sci.* **2021**, *9*, 6183−6202.
(8) Nel, A.; Xia, T.; Madler, L.; Li, N. Toxic Potential of Materials at the Nanolevel. *Science* **2006**, *311* (5761), 622−627.
(9) Li, G.; Sun, B.; Li, Y.; Luo, C.; He, Z.; Sun, J. Small-molecule Prodrug Nanoassemblies: An Emerging Nanoplatform for Anticancer Drug Delivery. *Small* **2021**, *17* (52), 2101460.
(10) Han, H.; Wang, H.; Jangili, P.; Li, M.; Wu, L.; Zang, Y.; Sedgwick, A.; Li, J.; He, X.; James, T.; Kim, J. The Design of Small-molecule Prodrugs and Activatable Phototherapeutics for Cancer Therapy. *Chem. Soc. Rev.* **2023**, *52*, 879.
(11) Li, H.; Zang, W.; Mi, Z.; Li, J.; Wang, L.; Xie, D.; Zhao, Li; Wang, D. Tailoring Carrier-free Nanocombo of small-molecule prodrug for Combinational Cancer Therapy. *J. Controlled Release* **2022**, *352*, 256−275.
(12) Ma, S.; Kim, J.; Chen, W.; Li, L.; Lee, J.; Xue, J.; Liu, Y.; Chen, G.; Tang, B.; Tao, W.; Kim, J. Cancer Cell-Specific Fluorescent Prodrug Delivery Platforms. *Adv. Sci.* **2023**, *10*, 2207768.
(13) Ye, J.; Wu, J.; Liu, B. Therapeutic Strategies of Dual-target Small Molecules to Overcome Drug Resistance in Cancer Therapy. *BBA-Rev. Cancer.* **2023**, *1878*, 188866.
(14) Wang, J.; Zhang, J.; Wang, J.; Hu, X.; Ouyang, L.; Wang, Y. Small-Molecule Modulators Targeting Toll-like Receptors for Potential Anticancer Therapeutics. *J. Med. Chem.* **2023**, *66*, 6437−6462.
(15) Huang, P.; Wang, D.; Su, Y.; Huang, W.; Zhou, Y.; Cui, D.; Zhu, X.; Yan, D. Combination of Small Molecule Prodrug and Nanodrug Delivery: Amphiphilic Drug−Drug Conjugate for Cancer Therapy. *J. Am. Chem. Soc.* **2014**, *136*, 11748−11756.
(16) Lammers, T.; Aime, S.; Hennink, W. E.; Storm, G.; Kiessling, F. Theranostic Nanomedicine. *Acc. Chem. Res.* **2011**, *44* (10), 1029−1038.
(17) Muthu, M. S.; Leong, D. T.; Mei, L.; Feng, S. S. Nanotheranostics-Application and Further Development of Nanomedicine Strategies for Advanced Theranostics. *Theranostics* **2014**, *4* (6), 660−677.
(18) Wang, B.; Liu, S.; Liu, X.; Hu, R.; Qin, A.; Tang, B. Z. Aggregation-Induced Emission Materials that Aid in Pharmaceutical Research. *Adv. Healthc. Mater.* **2021**, *10* (24), 2101067.
(19) Mazrad, Z. A. I.; Lee, K.; Chae, A.; In, I.; Lee, H.; Park, S. Y. Progress in Internal/External Stimuli Responsive Fluorescent Carbon Nanoparticles for Theranostic and Sensing Applications. *J. Mater. Chem. B* **2018**, *6* (8), 1149−1178.
(20) Mao, D.; Liu, B. Biology-Oriented Design Strategies of AIE Theranostic Probes. *Matter* **2021**, *4*, 350−376.
(21) Zuo, Y.; Shen, H.; Sun, F.; Li, P.; Sun, J.; Kwok, R. T. K.; Lam, J. W. Y.; Tang, B. Z. Aggregation-Induced Emission Luminogens for Cell Death Research. *ACS Bio. & Med. Chem. Au* **2022**, *2*, 236.
(22) Yuan, Y.; Liu, B. Visualization of Drug Delivery Processes Using AIEgens. *Chem. Sci.* **2017**, *8*, 2537−2546.
(23) Leung, N. L. C.; Xie, N.; Yuan, W.; Liu, Y.; Wu, Q.; Peng, Q.; Miao, Q.; Lam, J. W. Y.; Tang, B. Z. (2014). Restriction of intramolecular motions: the general mechanism behind aggregation-induced emission. *Chem. − Eur. J.* **2014**, *20*, 15349−15353.
(24) Zhao, Z.; Lam, J. W. Y.; Tang, B. Z. Tetraphenylethene: a Versatile AIE Building Block for the Construction of Efficient Luminescent Materials for Organic Light-Emitting Diodes. *J. Mater. Chem.* **2012**, *22*, 23726−23740.
(25) Zhang, H.; Tang, B. Z. Through-Space Interactions in Clusteroluminescence. *JACS Au* **2021**, *1*, 1805−1814.
(26) Liu, J.; Zhang, H.; Hu, L.; Wang, J.; Lam, J. W. Y.; Blancafort, L.; Tang, B. Z. Through-Space Interaction of Tetraphenylethylene: What, Where, and How. *J. Am. Chem. Soc.* **2022**, *144*, 7901−7910.
(27) La, D. D.; Bhosale, S. V.; Jones, L. A.; Bhosale, S. V. Tetraphenylethylene-Based AIE-Active Probes for Sensing Applications. *ACS Appl. Mater. Interfaces* **2018**, *10*, 12189−12216.
(28) Yan, S.; Sun, P.; Niu, N.; Zhang, Z.; Xu, W.; Zhao, S.; Wang, L.; Wang, D.; Tang, B. Z. One Stone, Four Birds" Ion Engineering to Fabricate Versatile Core−Shell Organosilica Nanoparticles for Intelligent Nanotheranostics. *ACS Nano* **2022**, *16* (6), 9785−9798.
(29) Hu, X.; Sedgwick, A.; Mangel, D.; Shang, Y.; Steinbrueck, A.; Yan, K.; Zhu, L.; Snelson, D.; Sen, S.; Chau, C.; Juarez, G.; Lynch, V.; He, X.; Sessler, J. Tuning the Solid-and Solution-state Fluorescence of the Iron-chelator Deferasirox. *J. Am. Chem. Soc.* **2022**, *144* (16), 7382−7390.
(30) Chu, B.; Qu, Y.; He, X.; Hao, Y.; Yang, C.; Yang, Y.; Hu, D.; Wang, F.; Qian, Z. ROS-responsive Camptothecin Prodrug Nanoparticles for On-demand Drug Release and Combination of Chemotherapy and Photodynamic Therapy. *Adv. Funct. Mater.* **2020**, *30* (52), 2005918.
(31) Chen, K.-F.; Zhang, Y.; Lin, J.; Chen, J.-Y.; Lin, C.; Gao, M.; Chen, Y.; Liu, S.; Wang, L.; Cui, Z.-K.; Jia, Y.-G. Upper Critical Solution Temperature Polyvalent Scaffolds Aggregate and Exterminate Bacteria. *Small* **2022**, *18*, 2107374.
(32) Song, Y.; Zhang, H.; Wang, X.; Geng, X.; Sun, Y.; Liu, J.; Li, Z. One Stone, Three Birds: pH Triggered Transformation of Aminopyronine and Iminopyronine Based Lysosome Targeting Viscosity Probe for Cancer Visualization. *Anal. Chem.* **2021**, *93*, 1786−1791.
(33) Yao, L.; Zhao, M.-M.; Luo, Q.-W.; Zhang, Y.-C.; Liu, T.-T.; Yang, Z.; Liao, M.; Tu, P.; Zeng, K.-W. Carbon Quantum Dots-Based Nanozyme from Coffee Induces Cancer Cell Ferroptosis to Activate Antitumor Immunity. *ACS Nano* **2022**, *16* (6), 9228−9239.
(34) Swietach, P. What is pH Regulation, and Why do Cancer Cells Need It? *Cancer Metast Rev.* **2019**, *38*, 5−15.
(35) Li, Y.; Wu, X.; Yang, B.; Zhang, X.; Li, H.; Umar, A.; De Rooij, N. F.; Zhou, G.; Wang, Y. Synergy of CO2 Response and

https://doi.org/10.1021/acsanm.3c03611
ACS Appl. Nano Mater. 2023, 6, 19807−19817

Aggregation-Induced Emission in a Block Copolymer: a Facile Way to "See" Cancer Cells. *ACS Appl. Mater. Interfaces* **2019**, *11*, 37077−37083.
(36) Leo, G.; Kala, S. Cellular pH gradient in tumor versus normal tissue: potential exploitation for the treatment of cancer. *Cancer Res.* **1996**, *56*, 1194−1198.
(37) Han, S.; Lee, J.; Jung, E.; Park, S.; Sagawa, A.; Shibasaki, Y.; Lee, D.; Kim, B.-S. Mechanochemical Drug Conjugation *via* pH-Responsive Imine Linkage for Polyether Prodrug Micelles. *ACS Appl. Bio. Mater.* **2021**, *4*, 2465−2474.
(38) Kalva, N.; Uthaman, S.; Lee, S. J.; Lim, Y. J.; Augustine, R.; Huh, K. M.; Park, I.-K.; Kim, I. Degradable pH-Responsive Polymer Prodrug Micelles with Aggregation-Induced Emission for Cellular Imaging and Cancer Therapy. *React. Funct. Polym.* **2021**, *166*, 104966.
(39) da Silva, C. M.; da Silva, D. L.; Modolo, L. V.; Alves, R. B.; de Resende, M. A.; Martins, C. V.B.; de Fatima, A. Schiff Bases: a Short Review of Their Antimicrobial Activities. *J. Adv. Res.* **2011**, *2* (1), 1−8.
(40) Wu, J.-S.; Liu, W.-M.; Zhuang, X.-Q.; Wang, F.; Wang, P.-F.; Tao, X.-H.; Wu, S.-K.; Lee, S.-T. Fluorescence Turn on of Coumarin Derivatives by Metal Cations: a New Signaling Mechanism Based on C= N Isomerization. *Org. Lett.* **2007**, *9*, 33−36.
(41) Wu, J.; Liu, W.; Ge, J.; Zhang, H.; Wang, P. New Sensing Mechanisms for Design of Fluorescent Chemosensors Emerging in Recent Years. *Chem. Soc. Rev.* **2011**, *40*, 3483−3495.
(42) Lu, G.; Middleton, R.; Sun, H.; Naniong, M.; Ott, C.; Mitsiades, C.; Wong, K.; Bradner, J.; Kaelin, W., Jr The Myeloma Drug Lenalidomide Promotes the Cereblon-Dependent Destruction of Ikaros Proteins. *Science* **2014**, *343* (6168), 305−309.
(43) Krönke, J.; Udeshi, N.; Narla, A.; Grauman, P.; Hurst, S.; McConkey, M.; Svinkina, T.; Heckl, D.; Comer, E.; Li, X.; Ciarlo, C.; Hartman, E.; Munshi, N.; Schenone, M.; Schreiber, S.; Carr, S.; Ebert, B. Lenalidomide Causes Selective Degradation of IKZF1 and IKZF3 in Multiple Myeloma Cells. *Science* **2014**, *343* (6168), 301−305.
(44) Ueno, T.; Urano, Y.; Setsukinai, K.; Takakusa, H.; Kojima, H.; Kikuchi, K.; Ohkubo, K.; Fukuzumi, S.; Nagano, T. Rational Principles for Modulating Fluorescence Properties of Fluorescein. *J. Am. Chem. Soc.* **2004**, *126* (43), 14079−14085.
(45) Zhang, X.; Chi, L.; Ji, S.; Wu, Y.; Song, P.; Han, K.; Guo, H.; James, T.; Zhao, J. Rational Design of d-PeT Phenylethynylated-carbazole Monoboronic Acid Fluorescent Sensors for the Selective Detection of α-hydroxyl Carboxylic Acids and Monosaccharides. *J. Am. Chem. Soc.* **2009**, *131* (47), 17452−17463.
(46) Lee, H.; Hancock, R.; Lee, H. Role of Fluorophore−metal Interaction in Photoinduced Electron Transfer (PET) Sensors: Time-dependent Density Functional Theory (TDDFT) study. *J. Phys. Chem. A* **2013**, *117* (50), 13345−13355.
(47) Mai, Z.; Li, H.; Gao, Y.; Niu, Y.; Li, Y.; de Rooij, N. F.; Umar, A.; Al-Assiri, M. S.; Wang, Y.; Zhou, G. Synergy of CO2-response and Aggregation Induced Emission in a Small Molecule: Renewable Liquid and Solid CO2 Chemosensors with High Sensitivity and Visibility. *Analyst* **2020**, *145*, 3528−3534.
(48) Semichem, Inc. *GaussView 6.0.16 program*; http://gaussian.com/gaussview6/ (accessed on Nov 25, 2019).
(49) Zhao, Y.; Truhlar, D. G. The M06 Suite of Density Functionals for Main Group Thermochemistry, Thermochemical Kinetics, Noncovalent Interactions, Excited States, and Transition Elements: Two New Functionals and Systematic Testing of Four M06-class Functionals and 12 Other Functionals. *Theor. Chem. Acc.* **2008**, *120*, 215−241.
(50) Weigend, F.; Ahlrichs, R. Balanced Basis Sets of Split Valence, Triple Zeta Valence and Quadruple Zeta Valence Quality for H to Rn: Design and Assessment of Accuracy. *Phys. Chem. Chem. Phys.* **2005**, *7*, 3297−3305.
(51) Devlin, F.; Stephens, P.; Cheeseman, J.; Frisch, M. Ab initio prediction of vibrational absorption and circular dichroism spectra of chiral natural products using density functional theory: camphor and fenchone. *J. Phys. Chem. A* **1997**, *101* (35), 6322−6333.
(52) Hehre, W. Ab initio molecular orbital theory. *Acc. Chem. Res.* **1976**, *9* (11), 399−406.
(53) Frisch, M.; Trucks, G.; Schlegel, H.; Scuseria, G.; Robb, M.; Cheeseman, J.; Scalmani, G.; Barone, V.; Petersson, G.; Nakatsuji, H. *Gaussian 16*, revision C. 01; Gaussian, Inc.: Wallingford, CT, 2016.
(54) Humphrey, W.; Dalke, A.; Schulten, K. VMD: Visual Molecular Dynamics. *J. Mol. Graph. Model.* **1996**, *14*, 33−38.
(55) Lu, T.; Chen, F. Multiwfn: a Multifunctional Wavefunction Analyzer. *J. Comput. Chem.* **2012**, *33* (5), 580−592.

https://doi.org/10.1021/acsanm.3c03611
ACS Appl. Nano Mater. 2023, 6, 19807−19817